Journal of Inorganic Biochemistry 169 (2017) 50–60

Contents lists available at ScienceDirect

Journal of Inorganic Biochemistry

journal homepage: www.elsevier.com/locate/jinorgbio

Challenges encountered during development of Mn porphyrin-based, potent redox-active drug and superoxide dismutase mimic, MnTnBuOE-2-PyP^{5+}, and its alkoxyalkyl analogues

Zrinka Rajic [a], Artak Tovmasyan [a], Otávio L. de Santana [b], Isabelle N. Peixoto [b], Ivan Spasojevic [c,d], Silmar A. do Monte [b], Elizete Ventura [b], Júlio S. Rebouças [b,*], Ines Batinic-Haberle [a,**]

[a] Department of Radiation Oncology, Duke University Medical Center, Durham, NC 27710, USA
[b] Departamento de Química, CCEN, Universidade Federal da Paraiba, João Pessoa, PB 58051-900, Brazil
[c] Department of Medicine, Duke University Medical Center, Durham, NC 27710, USA
[d] Duke Cancer Institute, Pharmaceutical Research Shared Resource, PK/PD Core Laboratory, Durham, NC 27710, United States

ARTICLE INFO

Article history:
Received 26 August 2016
Received in revised form 21 December 2016
Accepted 3 January 2017
Available online 5 January 2017

Keywords:
SOD mimics
Alkoxyalkyl tosylates
Mn *N*-alkoxyalkylpyridylporphyrins
MnTnBuOE-2-PyP^{5+} (BMX-001)
MnTTEG-2-PyP^{5+}
FP-15
Mechanism of pyridyl nitrogen quaternization

ABSTRACT

We disclose here the studies that preceded and guided the preparation of the metal-based, redox-active therapeutic Mn(III) *meso*-tetrakis(*N*-n-butoxyethylpyridyl)porphyrin, MnTnBuOE-2-PyP^{5+} (BMX-001), which is currently in Phase I/II Clinical Trials at Duke University (USA) as a radioprotector of normal tissues in cancer patients. *N*-substituted pyridylporphyrins are ligands for Mn(III) complexes that are among the most potent superoxide dismutase mimics thus far synthesized. To advance their design, thereby improving their physical and chemical properties and bioavailability/toxicity profiles, we undertook a systematic study on placing oxygen atoms into *N*-alkylpyridyl chains via alkoxyalkylation reaction. For the first time we show here the unforeseen structural rearrangement that happens during the alkoxyalkylation reaction by the corresponding tosylates. Comprehensive experimental and computational approaches were employed to solve the rearrangement mechanism involved in quaternization of pyridyl nitrogens, which, instead of a single product, led to a variety of mixed *N*-alkoxyalkylated and *N*-alkylated pyridylporphyrins. The rearrangement mechanism involves the formation of an intermediate alkyl oxonium cation in a chain-length-dependent manner, which subsequently drives differential kinetics and thermodynamics of competing *N*-alkoxyalkylation versus *in situ* *N*-alkylation. The use of alkoxyalkyl tosylates, of different length of alkyl fragments adjacent to oxygen atom, allowed us to identify the set of alkyl fragments that would result in the synthesis of a single compound of high purity and excellent therapeutic potential.

1. Introduction

Cationic Mn(III) porphyrins are among the most efficacious superoxide dismutase (SOD) mimics and redox-active experimental therapeutics for the treatment of diseases associated with a disturbed cellular redox environment, commonly described as a state of oxidative stress [1–8]. Among *N*-alkylsubstituted pyridyl- or imidazolyl Mn porphyrins, their *ortho* isomers are the most studied compounds *in vitro*

Abbreviations: SOD, superoxide dismutase; $O_2^{\cdot-}$, superoxide; MnP, Mn porphyrin; MnTM-2-PyP^{5+}, AEOL10112, Mn(III) *meso*-tetrakis(*N*-methylpyridinium-2-yl)porphyrin (AEOL originates from the name of pharmaceutical company (which in turn got it name from the Aeolian islands in Sicilly, Italy), Aeolus Pharmaceuticals); MnTE-2-PyP^{5+} (AEOL10113, BMX-010, FBC-007 BMX originates from pharmaceutical company, BioMimetix JVLLC), Mn(III) *meso*-tetrakis(*N*-ethylpyridinium-2-yl)porphyrin; MnTnHex-2-PyP^{5+}, Mn(III) *meso*-tetrakis(*N*-n-hexylpyridinium-2-yl)porphyrin; MnTnBuOE-2-PyP^{5+} (BMX-001), Mn(III) *meso*-tetrakis(*N*-(n-butoxyethyl)pyridinium-2-yl)porphyrin; MnTDE-2-ImP^{5+}, AEOL10150, Mn(III) tetrakis(*N*,*N*′-diethylimidazolium-2-yl)porphyrin; MnTTEG-2-PyP^{5+}, Mn(III) *meso*-tetrakis[N-(1-[2-(2[-2-methoxy]ethoxy)ethoxy]ethyl)pyridinium-2-yl]porphyrin; FP15 (FeTTEG-2-PyP^{5+}), Fe(III) *meso*-tetrakis[N-(1-[2-(2[-2-methoxy]ethoxy)ethoxy]ethyl)pyridinium-2-yl]porphyrin; MnTAlkyl-2(3 or 4)-PyP, Mn(III) *meso*-tetrakis(*N*-alkylpyridinium-2(3 or 4)-yl)porphyrins—2, 3 and 4 relate to *ortho*, *meta* and *para* isomers respectively, alkyl being ethyl to n-hexyl; MnTAlkoxyalkyl-2-PyP^{5+}, Mn(III) *meso*-tetrakis(*N*-alkoxyalkylpyridinium-2-yl)porphyrins; MnTAlkoxyalkyl-3-PyP^{5+}, Mn(III) *meso*-tetrakis(*N*-alkoxyalkylpyridinium-3-yl)porphyrins; MnTAlkoxyalkyl-4-PyP^{5+}, Mn(III) *meso*-tetrakis(*N*-alkoxyalkylpyridinium-4-yl)porphyrins — alkoxy relates to methoxy or n-butoxy, and alkyl varied from ethyl to n-hexyl; TS, transition state; EtOAc, ethyl acetate; DMF, *N*,*N*-dimethylformamide; TLC, thin layer chromatography; R_f, TLC retention factor; HFBA$^-$, heptafluorobutyrate anion; Ts, tosylate.

* Corresponding author.
** Correspondence to: I. Batinic-Haberle, Department of Radiation Oncology-Cancer Biology, Duke University Medical Center, Research Drive, 281b/285 MSRB I, Box 3455, Durham, NC 27710, USA.
E-mail addresses: jsreboucas2@gmail.com, jsreboucas@quimica.ufpb.br (J.S. Rebouças), ibatinic@duke.edu (I. Batinic-Haberle).

http://dx.doi.org/10.1016/j.jinorgbio.2017.01.003
0162-0134/

and *in vivo*. These include Mn(III) *meso*-tetrakis(*N*-ethylpyridinium-2-yl)porphyrins (MnTE-2-PyP^{5+}, AEOL10113, BMX-010), Mn(III) *meso*-tetrakis(*N*,*N*′-diethylimidazolium-2-yl)porphyrin (MnTDE-2-ImP^{5+}, AEOL10150), Mn(III) *meso*-tetrakis(*N*-n-hexylpyridinium-2-yl)porphyrin (MnTnHex-2-PyP^{5+}), and, more recently, Mn(III) *meso*-tetrakis(*N*-n-butoxyethylpyridinium-2-yl)porphyrin (MnTnBuOE-2-PyP^{5+}, BMX-001) (Fig. 1) [1–8]. Their design, properties, mechanisms of actions, and therapeutic effects (such as injuries of central nervous system, diabetes, cancer, radioprotection, etc. [1,2,4–6]) have been the subject of several recent reviews [4–6].

The development of redox-active therapeutics has paralleled the advances in synthesis of powerful SOD mimics [1–8]. Mn(III) 2-*N*-alkylpyridylporphyrins emerged as potent SOD mimics, some of which approaching the activity of SOD enzymes [5]. Whereas the intrinsic antioxidant potency of Mn porphyrins (MnPs) is physico-chemically controlled, their biological activity relies also on their toxicity, and bioavailability, which, in turn, depends on factors such as size and lipophilicity. The understanding of key structural features of MnPs in controlling intrinsic SOD activity [4,9,10], compound stability [10], lipophilicity [11,12], bioavailability [13–16], subcellular localization [17–19], and pharmacokinetics [15,16] have paved the way to the optimization of other related compounds [5,20,21].

The optimization of MnP-based therapeutics has been actively sought by the controlled modification of the side-chain pyridinium moieties. Short alkyl-chained analogues, such as MnTE-2-PyP^{5+}, are of low lipophilicity and therefore low availability to brain tissue, which limits its use in the treatment of central nervous system disorders. Nonetheless, successful pre-clinical profile of the short alkyl-chained derivative MnTE-2-PyP^{5+} in a series of disease models [5,6,22] has forwarded it into Phase I/II Clinical Trials in Canada. Long alkyl-chained analogues, such as MnTnHex-2-PyP^{5+}, accumulate in cells at higher levels than their ethyl analogue. Yet, systemic administration of the lipophilic *N*-alkylpyridylporphyrins is hampered by toxicity associated with their surfactant/micellar properties. As an attempt to reduce the surfactant character brought by the long alkyl side chains, a strategy of replacing a CH_2 group of the alkyl chains by oxygen atoms to yield alkoxyalkyl analogues was envisaged. Yet the actual execution of such approach was troublesome.

We describe herein the pitfalls that hampered those studies and the experimental and computational studies that eventually guided us into the development of remarkable SOD mimic - MnTnBuOE-2-PyP^{5+} (Fig. 1) [54]. The notable biological efficiency and safe toxicity profile (e.g., lack of genotoxicity in a rat Comet assay) of MnTnBuOE-2-PyP^{5+} in pre-clinical studies [6,23] have justified its pursue toward clinics; indeed, MnTnBuOE-2-PyP^{5+} is now in Phase I/II Clinical Trials at Duke University (USA) on glioma patients (NCT02655601) as a radioprotector of normal brain and will enter soon another trial on radioprotection of salivary glands and mouth mucosa with head & neck cancer patients [24]. More specifically, we show herein that the impurities hampering the development of oxygenated side-chain MnPs, such as methoxyalkyl (MOalkyl) derivatives (alkyl = Et, n-Bu, n-Pen, and n-Hex) of *ortho*, *meta*, and *para* Mn(III) *N*-pyridylporphyrins relate to the unexpected formation of *methyl*-containing MnPs. The extent of contamination varied with the length of the methoxyalkyl chains and limited severely the use of some of the methoxyalkyl constructs, as separation of methyl- and methoxyalkyl-containing species is difficult. This, in turn, compromises biological testing of the samples. Understanding of the nature and origin of these impurities, which plagued all methoxyalkyl MnP preparations, will facilitate future synthetic endeavors in the field of lipophilic, non-toxic MnP-based therapeutics. The mechanism associated with competing methylation/methoxyalkylation reactions was studied by Density Functional Theory at the M06-2X level and correlated well with the experimental data. The overall results presented here call for a reevaluation of the previously published PEG and methoxyalkyl data on both Fe(III) and Mn(III) porphyrins, such as FP-15, MnTTEG-2-PyP^{5+}, and MnTMOE-2-PyP^{5+} [25,26].

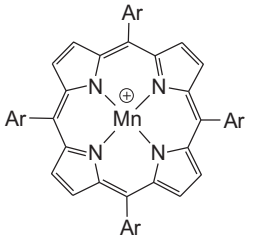

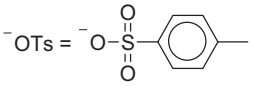

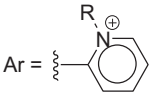

***ortho* systems: Alkyl series**

MnTM-2-PyP^{5+}: R = Me
MnTE-2-PyP^{5+}: R = Et
MnTnBu-2-PyP^{5+}: R = n-Bu
MnTnHex-2-PyP^{5+}: R = n-Hex

***ortho* systems: Alkoxyalkyl series**

MnTMOE-2-PyP^{5+}: R = $MeOCH_2CH_2$-
MnTMOBu-2-PyP^{5+}: R = $MeOCH_2(CH_2)_2CH_2$-
MnTMOPen-2-PyP^{5+}: R = $MeOCH_2(CH_2)_3CH_2$-
MnTMOHex-2-PyP^{5+}: R = $MeOCH_2(CH_2)_4CH_2$-
MnTnBuOE-2-PyP^{5+}: R = $nBuOCH_2CH_2$-
MnTnHexOE-2-PyP^{5+}: R = $nHexOCH_2CH_2$-
MnTTEG-2-PyP^{5+}: R = $MeOCH_2CH_2OCH_2CH_2OCH_2CH_2$-

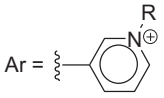

***meta* systems: Alkyl series**

MnTM-3-PyP^{5+}: R = Me

***meta* systems: Alkoxyalkyl series**

MnTMOE-3-PyP^{5+}: R = $MeOCH_2CH_2$-
MnTMOBu-3-PyP^{5+}: R = $MeOCH_2(CH_2)_2CH_2$-
MnTMOPen-3-PyP^{5+}: R = $MeOCH_2(CH_2)_3CH_2$-
MnTMOHex-3-PyP^{5+}: R = $MeOCH_2(CH_2)_4CH_2$-

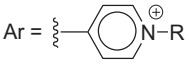

***para* systems: Alkyl series**

MnTM-4-PyP^{5+}: R = Me

***para* systems: Alkoxyalkyl series**

MnTMOE-4-PyP^{5+}: R = $MeOCH_2CH_2$-
MnTMOBu-4-PyP^{5+}: R = $MeOCH_2(CH_2)_2CH_2$-
MnTMOPen-4-PyP^{5+}: R = $MeOCH_2(CH_2)_3CH_2$-
MnTMOHex-4-PyP^{5+}: R = $MeOCH_2(CH_2)_4CH_2$-

Fig. 1. Structures of Mn(III) porphyrins relevant to this work.

2. Materials and methods

2.1. Reagents

H_2T-2-PyP, H_2T-3-PyP and H_2T-4-PyP were purchased from Frontier Scientific, 2-Methoxyethyl tosylate (>98%), 4-methoxybuthanol (>98%), 6-bromohexan-1-ol (>95%), from TCI America, 5-methoxypenthanol (98%) from Karl Industries Inc., *p*-toluenesulfonyl chloride (98%) from Alpha Aesar, pyridine (99%) and tetra-n-butylammonium chloride hydrate (98%) from Aldrich, $MnCl_2 \times 4H_2O$ (99.7%) and hexane from J. T. Baker and NH_4PF_6 (99.99% pure) from GFS chemicals. Anhydrous diethyl ether and acetone were from EMD chemicals; absolute methanol, ethyl acetate (EtOAc), dichloromethane, chloroform, acetonitrile, EDTA and KNO_3 were from Mallinckrodt; 98% anhydrous *N,N*-dimethylformamide (DMF, kept over 4-Å molecular sieves), plastic-backed silica gel thin layer chromatography (TLC) plates (Z122777-25EA) were from Sigma-Aldrich; and silica (SiliaFlash® G60, 70–230 mesh) was from SiliCycle (Canada). 6-Methoxyhexan-1-ol and H_2TMOE-2-PyP^{4+} were prepared as previously described [26,27]. All other chemicals were used as received.

2.2. 4-Methoxybutyl, 5-methoxypentyl, and 6-methoxyhexyl tosylates

Syntheses were carried out as described earlier [28,29]. In short, to a 50 mL $CHCl_3$ solution containing 0.048 mol of the appropriate methoxyalcohol (4-methoxybutanol: 5.00 g; 5-methoxypentanol: 5.67 g; 6-methoxyhexanol: 6.40 g) at 0 °C, pyridine (7.76 mL, 0.096 mol) was added, followed by the dropwise addition of a 50 mL $CHCl_3$ solution of *p*-toluenesulfonyl chloride (13.73 g, 0.072 mol). The reaction mixture was stirred at 0 °C for 2 h (for 4-metoxybutanol and 5-methoxypentanol) or 4.5 h (for 6-methoxyhexanol). After extraction with H_2O (4 × 100 mL), 2 M HCl (4 × 100 mL), saturated $NaHCO_3$ solution (till pH ~ 6) and H_2O (3 × 100 mL), the organic phase was dried with anhydrous Na_2SO_4 and filtered. The solution was evaporated in a rotary evaporator and the oily residue was purified by flash chromatography (CombiFlash instrument, mobile phase = Hex:EtOAc). The fractions contained the desired product were combined and evaporated on a rotary evaporator to yield a colorless oil. ^{1}H, ^{13}C NMR, and MS data were in agreement with the proposed structures. The MS spectra and NMR data of 4-methoxybutyl tosylate, 5-methoxypentyl tosylate and 6-methoxyhexyl tosylate are provided in Supplementary Information, Fig. S1 (A-C) and Table S1. Yield: 4-methoxybutyl tosylate: 84.7% (10.50 g); 5-methoxypentyl tosylate: 76.7% (10.03 g); 6-methoxyhexyl tosylate: 90% (12.37 g).

2.3. Mn porphyrins

The methoxyalkylation of H_2T-X-PyP (X = 2, 3, or 4) and the subsequent Mn metallation to prepare MnTMOE-X-PyPCl_5, MnTMOBu-X-PyPCl_5, MnTMOPen-X-PyPCl_5, and MnTMOHex-X-PyPCl_5 (X = 2, 3, or 4) were carried out as previously described for other related alkyl systems [30]. To a solution of H_2T-X-PyP (X = 2, 3, or 4) (20 mg, 0.032 mmol) in anhydrous DMF (2 mL, preheated at 105 °C for 15 min) the appropriate tosylate was added (2-methoxyethyl tosylate, MeOEtOTs: 3.67 g, 0.016 mol; 4-methoxybutyl tosylate, MeOBuOTs: 4.18 g, 0.016 mol; 5-methoxypentyl tosylate, MeOPenOTs: 4.00 g, 0.016 mol; 6-methoxyhexyl *p*-tosylate, MeOHexOTs: 2.20 g, 0.008 mol). The course of the reaction was followed by TLC, using 1:1:8 KNO_3-saturated H_2O:H_2O:acetonitrile as mobile phase. The reaction mixture was filtrated into a separatory funnel containing H_2O and chloroform and extracted several times with chloroform. The isolation of chloride salt, the metalation with $MnCl_2$ and the isolation of Mn porphyrin as chloride salt was carried out as previously described for Mn(III) *N*-alkylpyridylporphyrins [30]. The products were dried under vacuum at room temperature. Isolated solids were labeled "methoxyalkyl chain/porphyrin isomer" according to the starting methoxyalkyl tosylate and porphyrin used; a short form was used for both the tosylates (*i.e.*, MeOEt, MeOBu, MeOPen, MeOHex) and porphyrin isomer (2-Py, 3-Py, and 4-Py standing for *ortho*, *meta*, and *para* *N*-pyridylporphyin systems), respectively. Drying the solids at high temperature was not attempted in order to avoid likely thermal dealkylation, as reported previously for related MnTE-2-PyP^{5+} [31]. It is worth noting that TLC and ESI-MS analyses indicate that solids were fully quaternized but were not single compounds (see Results and Discussion Section).

2.4. Analysis of the Mn complexes

Electrochemistry, electrospray-ionization mass spectrometry (ESI-MS), UV–visible spectroscopy and SOD-like activity were carried out as previously described [29,32]. All quantum chemistry calculations have been performed at the M06-2X/6–311++G(2d,p)//M06-2X/6–31+G(d) DFT level [33–38] using Gaussian 09 software [39]. All frequency calculations were carried out at 105 °C and used to characterize minima and transition states (TS). The solvent effect has been taken into account using the CPCM continuum solvation model [40] for *N,N*-dimethylformamide (DMF). The free energies of reactants, transition states, and products have been obtained from the ideal gas partition functions for the structures optimized in solution [40] and corrected to include the compression work of the gas [41] (or liberation free energy [42]) to standard 1 mol L^{-1} concentration. The coulombic stabilization energy due to the formation of ionic pairs in DMF has also been included in the final results by approximating each ion as a sphere, whose volume was considered the same as that of the solute cavity; [43] the distance between cation and anion in the ionic pair was taken as the sum of the two sphere radii.

3. Results and discussion

3.1. Quartenization of Mn(III) N-pyridylporphyrins with methoxyalkyl tosylates is compromised by competing in situ methylation

The introduction of oxygenated alkyl sidechains has been explored as a means to reduce the toxicity of Mn(III) *N*-alkylpyridylporphyrins. We describe here the synthetic drawbacks associated with this synthetic strategy. Gaining insights into the synthetic approaches benefited the development of MnTnBuOE-2-PyP^{5+} paving its pathway towards clinic. The methoxyalkylation of all three isomers of *N*-pyridylporphyrins was carried out with four tosylates of appropriate chain length (*i.e.*, MeOEtOTs, MeOBuOTs, MeOPenOTs, and MeOHexOTs), accounting for 12 preparations. The synthetic and purification routes were adapted from that of related alkyl derivatives [29,30,44] and involved the reaction of H_2T-X-PyP (X = 2, 3, or 4) with the appropriate tosylate in DMF at 105 °C followed by metallation with $MnCl_2$ under aqueous conditions at room temperature. None of the isolated solids appeared to be a single compound (see below). Of note, none of the isolated solids were subjected to heating in order to avoid thermal dequaternization [31].

Methoxyalkylation reactions were monitored by TLC. None of the preparations yielded a single TLC spot. Indeed, TLC plates showed that some preparations were a mixture of at least 5 products almost evenly distributed. Reactions were deemed complete when the starting porphyrin had been fully consumed and the resulting spotting profile did not change with time [30,32]. Whereas the presence of more than one TLC spot is common for *ortho* isomers bearing long alkyl chains (e.g., n-hexyl), as a result of them being a mixture of atropoisomers, a single TLC spot has always been observed in the case of *ortho* isomers with short alkyl chains (*e.g.*, methyl and ethyl), as well as for *meta* and *para* isomers, for which atropisomerism is not expected. The origin of TLC spots as a result of incomplete quaternization of MnPs [32], was ruled out based on the following evidences: (a) prolonged heating time and additional amounts of the methoxyalkylating reagents did not change the TLC profile; (b) the UV–vis spectra of the isolated

materials were characterized by a well-defined Soret band in a region expected for fully quaternized MnPs (partial quaternization would have shifted the Soret band to higher wavelengths); [10,32] (c) voltammograms of the isolated MnPs were symmetrical and with no shoulders, indicating either the presence of only one MnP species (which is not the case, given the TLC analyses), or that the sample contains a mixture of very closely related species with nearly identical Mn(III)/Mn(II) metal-centered reduction potential, $E_{1/2}$. A mixture of species of varying degree of quaternization (*i.e.*, partial quaternization) would have yielded ill-defined voltammograms [32], which was not observed in any of the preparations. A typical voltammogram (as commonly seen with this type of compounds [9]) is presented in Supplementary Information (Fig. S2) for the "MeOBu/3-Py" systems, for which 4 spots were clearly seen on TLC plates but voltammogram was well behaved.

The ESI-MS spectra under conditions that excluded MnP fragmentation [32] showed a set of peaks, typical of a mixture of compounds and consistent with TLC data. Heptafluorobutyrate anion ($HFBA^-$) was used as ion-pairing agent for ESI-MS analysis to facilitate multi-charged peak identification, as reported elsewhere [32]. Typical ESI-MS spectra are illustrated in Supplementary Information (Fig. S3) for the "MeOBu/3-Py" and "MeOBu/2-Py" systems, showing that all peaks in the *meta* system have a counterpart in the *ortho* system, and indicating that all products formed in the *meta* system have also an equivalent isomer in the *ortho* system. The ESI-MS spectra of all samples were characterized by two sets of peaks (Fig. 2). The first set ranging from *m/z* 385 to *m/z* 520 occurs in the region regularly associated with the ion-paired cluster $(MnP^{5+} + 2HFBA^-)^{3+}/3$, whereas the second set at *m/z* 685–890 relates to the ion-pair $(MnP^{5+} + 3HFBA^-)^{2+}/2$ [32]. Although the expected peaks corresponding to the fully quaternized methoxyalkylated species were observed in each case, these peaks were always accompanied by other peaks of lower *m/z* values and sometimes of greater intensity. A breakthrough in characterizing these systems was achieved by coupling the ESI-MS analysis with pre-separation of the samples by TLC-SiO_2 (sat. $KNO_{3(aq)}$:H_2O:CH_3CN, 1:1:8 v/v/v). Each TLC spot was isolated, and the MnP recovered from each TLC spot was individually analyzed by ESI-MS. As a typical case, TLC analysis of the "MeOBu/3-Py" material gave rise to 4 spots. Upon ESI-MS analysis 4 clean spectra characteristic of four MnP^{5+}-type compounds were obtained, whose spectral features, corresponding to the $(MnP^{5+} + 2HFBA^-)^{3+}/3$ ion-pairing region, are shown in Fig. 2. It is worth noting that each spectrum in Fig. 2 contains 1 of the four peaks in the *m/z* 385–520 region of the originally isolated sample; the same is true for other spectral regions (not shown). The ESI-MS data for each compound in Fig. 2 are consistent with a fully quaternized MnP^{5+} species (ion-paired with 2 $HFBA^-$ anions) in which both the number of methoxyalkyl moieties decreased from 4 to 1 and the number of methyl groups increased correspondingly from 0 to 3, maintaining the total number of substituents at the pyridyl moieties equals to four. The greater the number of methyl groups in the sample, the smaller the TLC retention factor (R_f) value, which was consistent with previous data on the increase in MnP^{5+} polarity (reduced

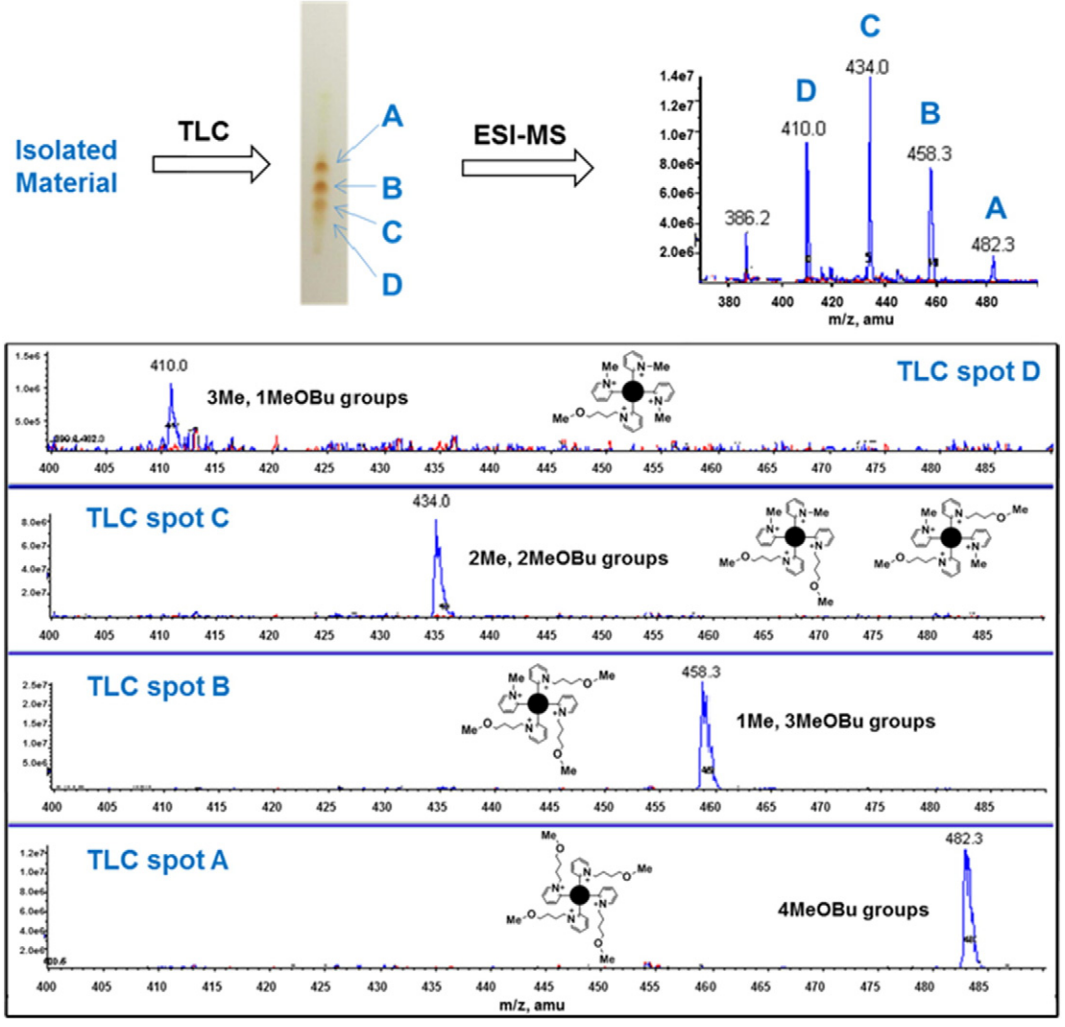

Fig. 2. TLC plate and ESI-MS analyses of both the crude mixture and the materials recovered from TLC spots of the "MeOBu/3-Py" system, which was initially thought to yield MnTMOBu-3-PyP^{5+}. TLC-SiO_2 was carried out in 1:1:8 = saturated KNO_3(aq):H_2O:CH_3CN system. ESI-MS peaks in the *m/z* 370–500 region correspond to ion-pairs $(MnP^{5+} + 2HFBA^-)^{3+}/3$.

lipophilicity) with decrease in length of pyridyl side-chain [11,12,30]. In the *meta* system, "MeOBu/3-Py" (Fig. 2), the extra peaks at *m/z* 386.2 and at *m/z* 685.5, correspond unambiguously to a well characterized compound containing no methoxybutyl groups at all, but 4 methyl groups instead, *i.e.*, MnTM-3-PyP^{5+} [32]. Similar scenario was seen with MeOBu/2-Py system (Fig. S3). It is worth noting that elemental analysis and C/N ratios of some of the isolated solids were surprisingly fine. Thus, based on elemental analysis, there was not a hint on how far away from a single compound some of the preparations were.

Considering that all MnP^{5+} species, regardless of the type of side-chain being methyl and/or methoxyalkyl, should share similar features related to ionization, ion-pairing, and ion suppression behavior [14, 16], the intensities of the peaks in the ESI-MS spectra were used as a crude measure of the contribution of each individual species to a whole isolated mixture. The distribution ratio of the desired tetramethoxyalkylated porphyrin against the side-products in which pyridyl groups had instead been quaternized by one, two, three, or four methyl groups in each of the 12 preparation is depicted in Fig. 3. The degree of overall methylation that took place in detriment of methoxyalkylation is presented in Fig. 4. The ESI-MS data in Fig. 2 agree with the relative color intensity of the TLC spots, as judged qualitatively by visual inspection. The examination of the distribution data (Fig. 3) and the degree of methylation *versus* methoxyalkylation (Fig. 4) indicated that the feasibility and extent of methylation varied with the nature of both the porphyrin isomer and the methoxyalkyl tosylate used. The general trends in these systems are summarized as it follows: (i) unwanted methylation is more pronounced in the *ortho* isomer systems than in the *meta* or the *para* ones; (ii) methoxyalkylation is favored (as opposed to methylation) by the use of MeOEtOTs and MeOHexOTs, whereas methylation prevails and the target tetramethoxyalkylated MnP is minimal with the use of MeOBuOTs and MeOPenOTs; (iii) methylation dominated the MeOPenOTs systems, with "MeOPen/X-Py" (X = 2, 3, or 4) solid being particularly rich in MnTM-X-PyP^{5+} species (X = 2, 3, or 4): the attempted methoxypentylation in the *ortho* system resulted in undesired MnTM-2-PyP^{5+} as the major compound in the isolated mixture! It is evident that methylation competes with methoxyalkylation. The source of the methyl groups in the reaction mixture and the mechanistic insights into this competition are addressed below.

As all pyridyl groups in any of the systems studied here have been quaternized to yield a mixture of MnP^{5+} species, the similarity of the electronic structure among these species renders their UV–vis and electrochemical features very much alike, which is consistent with UV–vis spectra and voltammograms that resemble the data improperly expected for a single pentacationic MnP compound. Additionally, it is evident that methylation competes with methoxyalkylation; the source of the methyl groups in the reaction mixture and some mechanistic insights into this competition will be addressed below.

3.2. Mechanistic investigations: competing methoxyalkylation versus methylation

The role of the methoxyalkyl tosylate as an *in situ* source of both the methoxyalkyl and the methyl groups was confirmed by experimental and computational data, which helped also to shed some light on the possible mechanism(s) responsible for the competing methoxyalkylation and methylation reactions.

Upon prolonged heating in neat DMF at 100–105 °C, *N*-pyridylporphyrins remained unchanged, which demonstrated that the source of methyl group was neither some impurity in the batches of the starting porphyrins, nor some compound generated *in situ* via thermal decomposition of DMF alone. This is consistent with the overwhelming data on the preparation of the corresponding *N*-alkylpyridylporphyrin series (alkyl = Et, nBu, nHex, nHep, etc), in which methylation has never been observed. It could be speculated that the methylation could arise from some process involving DMF decomposition under reaction conditions in the presence of the methoxyalkyl tosylates. To unambiguously rule out the involvement of DMF as a source of methyl groups, the quaternization reactions of H_2T-2-PyP with MeOBuOTs were carried out in deuterated DMF (d_6-DMF) and the ESI-MS product distribution profile of the isolated material was identical to that observed with non-deuterated DMF. Additionally, methylation did take place but peak isotopic shifts (expected if methylation had d_6-DMF as -CD_3 group source) were not observed, which reassured the methoxyakyl tosylates as *in situ* source of the methylation species.

Methoxyalkyl tosylates were thoroughly analyzed by ^{1}H and ^{13}C NMR spectroscopy, TLC and ESI-MS, and no impurities that could be responsible for methylation were detected. This supported a hypothesis in which the methylation species could be generated in situ via some thermal process in DMF. This would represent a porphyrin-independent path. Therefore the thermal stability of the methoxyalkyl tosylates was investigated under conditions similar to the ones used in porphyrin quaternization. Thus, methoxyalkyl tosylates were heated in DMF at 100 °C, while the transformations were monitored by TLC and ESI-MS. After 7 h heating, no changes were observed in the case of MeOEtOTs

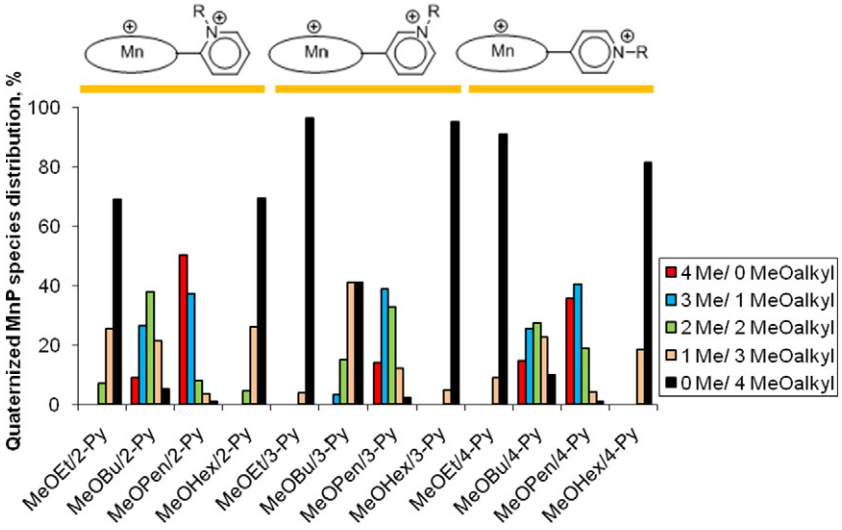

Fig. 3. The distribution of the mixture of species bearing "n" methoxyalkyl groups and "4-n" methyl groups (n = 0 to 4) on pyridyl nitrogens in different *N*-methoxyalkylpyridylporphyrin preparations.

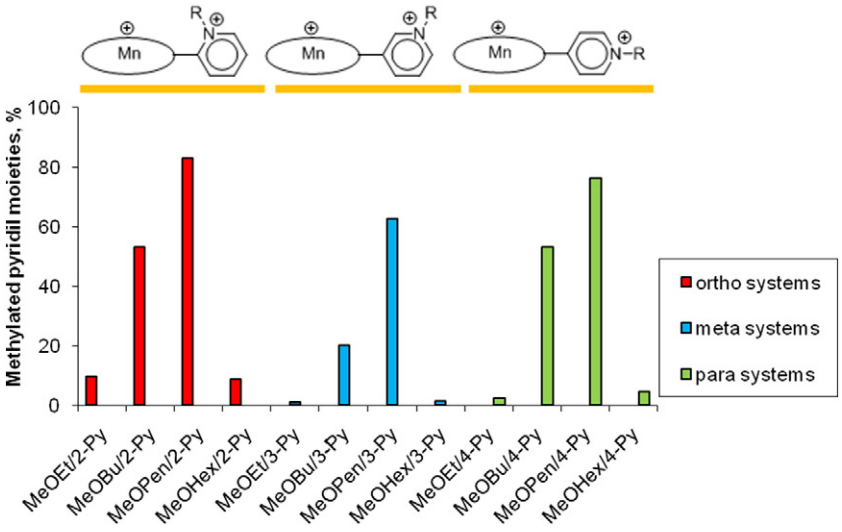

Fig. 4. The levels of overall methylation (as opposed to methoxyalkylation) in different *N*-methoxyalkylpyridylporphyrin preparations.

and MeOHexOTs. Conversely, a new product was clearly formed in the MeOBuOTs and MeOPenOTs cases. ESI-MS spectra of crude materials indicated the presence of a peak at *m/z* 187, which is consistent with the presence of methyl tosylate (MeOTs) in reaction mixture (Supplemental Information, Fig. S4). TLC co-elution of these materials with an authentic MeOTs sample confirmed the formation of MeOTs upon heating of MeOBuOTs and MeOPenOTs in DMF at 100 °C. Hence, the *in situ* formation of MeOTs could explain the competing methylation reactions observed during methoxyalkylation of the *N*-pyridylporphyrins.

The methoxyalkyl tosylates MeOBuOTs and MeOPenOTs were, as expected, more stable toward transformation into MeOTs at lower temperatures. At temperatures in the 60–80 °C range, MeOTs was detected upon heating of MeOBuOTs and MeOPenOTs in DMF for 45 h and 21 h, respectively. Although this information is of little importance for porphyrin methoxyalkylation itself (as methoxyalkylation, alike regular alkylation, is considerably slower at these temperatures, which would allow accumulation of MeOTs and thus methylation), it establishes that MeOBuOTs is more prone to transformation into MeOTs than MeOPenOTS. This relative propensity to yield MeOTs in situ correlates with the fact that methylation prevails in the MeOPenOTs systems compared to the MeOBuOTs systems (Fig. 3). Of note, MeOTs reacts significantly faster with *N*-pyridylporphyrins than its longer alkyl analogues, such as Et, nBu, nHex, etc.

It is clear that the MnP species distribution depicted in Fig. 3 arises from the balance between two competing reactions: methoxyalkylation and methylation. Additionally, the degree of methylation given in Fig. 4 is a result of a combination of various effects, such as, the availability of unquaternized pyridyl groups, the accumulation of the *in situ*-generated methylating agent, and the relative reactivity of the pyridyl group toward both the methoxyalkyl tosylate and the methylating agent. Three possible routes were conceived to accommodate the net transformations observed in these systems (Fig. 5). The mechanisms and reaction profiles of each route were studied computationally in order to shed some light on the dependence of the overall competing reactivity trends on both the *N*-pyridylporphyrin isomer and the length of the methoxyalkyl tosylate chain. The pyridyl moieties of the *N*-pyridylporphyrins were represented by a free pyridine ring in Fig. 5.The use of pyridine as a surrogate for pyridyl groups is justified by that fact that each of the four pyridyl groups in the *N*-pyridylporphyrins reacts independently of one another; such simplification allows for more accurate calculations.

Route A (Fig. 5) depicts the mechanism associated with the desired methoxyalkylation reaction, which is suggested to follow a regular S_N2 mechanism *via* a transition state (TS) $\mathbf{2_A}$ to yield the corresponding tosylate salt of methoxyalkylpyridinium (product **3a**). The methylation reaction certainly involves a rearrangement of the methoxyalkyl tosylate to yield the methylating agent *in situ*, for which two complimentary routes (B and C) were envisioned: the starting methoxyalkyl tosylate rearranges into a tosylate salt of a methyl oxonium cycloalkane as a common intermediate ($\mathbf{3_{B,C}}$) in both Routes B and C. This intermediate may, then, react directly with either pyridine (Route B) or tosylate (Route C). Route B explores the methylating properties of this oxonium salt, as there is literature precedent for alkylations carried out by trialkyloxonium salts [45]. In Route C, the tosylate salt of methyl oxonium cycloalkane rearranges further to yield the stable products MeOTs and the corresponding cyclic ether (products **5c**). The methylating agent in Route C is MeOTs, which reacts then with pyridine to yield the tosylate salt of methylpyridinium.

The quantum chemistry calculations on the mechanisms depicted in Fig. 5 have been performed at the DFT level using the M06-2X hybrid meta-generalized gradient approximation functional, which has shown good performance in thermochemistry, thermochemical kinetics, and non-covalent interaction studies of species that do not contain metals [46]. Single-point calculations with the 6–311++G(2d,p) basis set have been performed at the geometries optimized with the 6–31+G(d) basis set. Preliminary single-point calculations have also been performed with the smaller 6–311+G(d,p) basis set. There are no qualitative differences between the results obtained with the two basis sets, although changes of up to 6 kJ mol^{-1} between the two set of results have been observed. As all experimental reactions were carried out in DMF at 105 °C, all free energy data were calculated at this temperature using the CPCM continuum solvation model for DMF [40]. Use of a continuum solvation model is justified as specific solute-solvent interactions (*e.g.*, hydrogen bonds) are not expected in the studied systems. Additionally, CPCM model has shown good performance in studies of barrier heights and reaction energies of compounds in non-aqueous solutions [47–49]. The free energies of reactants, transition states and products are given in Fig. 6. These values include the compression work correction associated with moving a solute from a standard-state gas-phase concentration of 1 atm to a standard-state solution-phase concentration of 1 mol L^{-1} [41,42]. This effect is important for reactions or steps in which the molecularity between reactants and products is altered [50], such as in $\mathbf{1} \rightarrow \mathbf{2_A}$, $\mathbf{2_{B,C}} \rightarrow \mathbf{3_{B,C}}$, $\mathbf{4_B} \rightarrow \mathbf{5_B}$, $\mathbf{4_C} \rightarrow \mathbf{5_C}$, and $\mathbf{6_C} \rightarrow \mathbf{7_C}$ ($=\mathbf{5_B}$) steps, and accounts for a significant lowering of free energy changes (by ~10.8 kJ mol^{-1} at 105 °C). For MeOEtOTs the compression work effect leads to an increase of the energy difference between $\mathbf{2_{B,C}}$ and $\mathbf{2_A}$, while for MeOBuOTs and MeOPenOTs it leads to a decrease of this energy difference, but such decrease is not

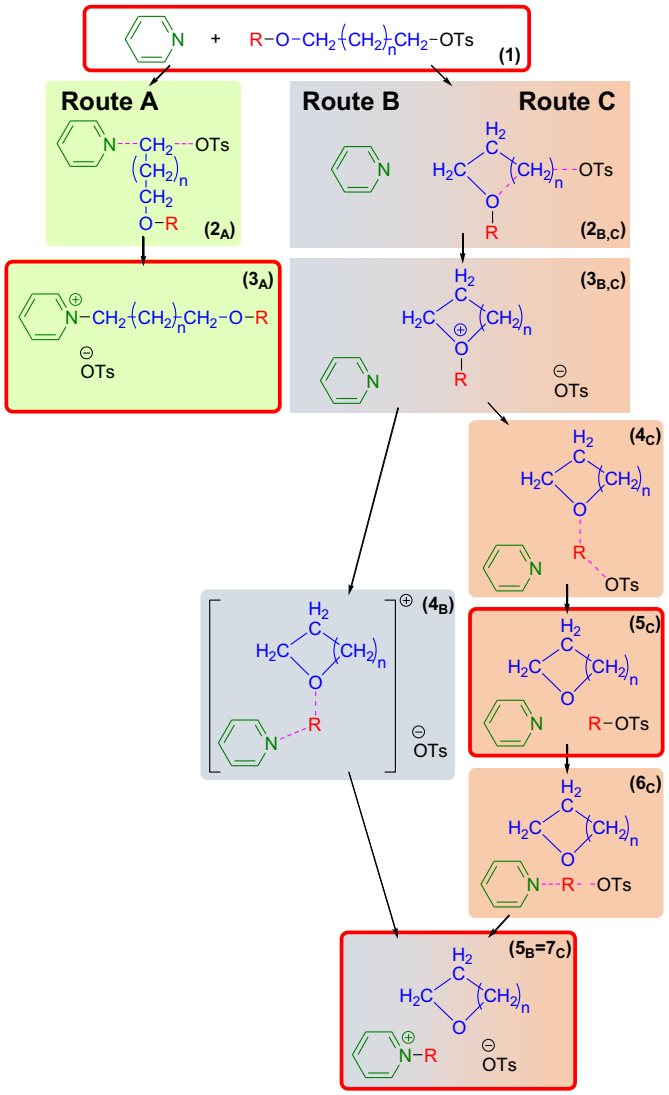

Fig. 5. Proposed reaction mechanisms for the competing alkoxyalkylation and methylation reactions of *N*-pyridylporphyrins in the presence of alkoxyalkyl tosylates. Pyridine has been used as a surrogate species for the pyridyl moieties of the *N*-pyridylporphyrins. R = methyl, and n = 0, 2, 3, or 4 for methoxyethyl, methoxybutyl, methoxypentyl or methoxyhexyl tosylates, respectively. R = butyl and n = 0 for butoxyethyl tosylate case.

enough to revert the energy ordering of $\mathbf{2_A}$ and $\mathbf{2_{B,C}}$. On the other hand, in the case of MeOHexOTs such effect causes a reversion in the energies of $\mathbf{2_{B,C}}$ and $\mathbf{2_A}$ (Fig. 6). The coulombic stabilization energy due to the formation of ionic pairs, as in $\mathbf{3_A}$, $\mathbf{3_{B,C}}$, $\mathbf{4_B}$ and $\mathbf{5_B}$, were of ~5 kJ mol^{-1}; and such correction had little impact on the overall free energy profile.

Routes B and C are marked by the involvement or formation of oxacycloalkanes as transition states, intermediates, or products. MeOEtOTs, MeOBuOTs, MeOPenOTs, and MeOHexOTs are, thus, associated with the corresponding heterocyclic rings oxacyclopropane (oxirane, epoxide), oxacyclopentane (oxolane, tetrahydrofuran), oxacyclohexane (oxane, tetrahydropyran), and oxacycloheptane (oxepane), respectively. Whereas Fig. 4 shows that the methylation of *N*-pyridylporphyrins, regardless of the isomer type, is favored in the following order MeOPetOTs > MeOBuOTs > MeOHexOTs > MeOEtOTs, it is worth noting that this overall reactivity correlates roughly with the stability trend of the corresponding heterocycles tetrahydropyran (6-membered ring) > tetrahydrofuran (5-membered ring) ≈ oxepane (7-membered ring) ≫ epoxide (3-membered ring) [51], with the exception being the MeOHexOTs system, which shows levels of methylation similar to those of MeOEtOTs (Fig. 4); this apparent incongruity will be dealt later. For the MeOEtOTs system, in which methylation by either Routes B or C depends on the formation of unstable 3-member ring species, the direct methoxyalkylation (Route A) is considerably more favorable (by >39 kJ mol^{-1}) than the other routes (compare the energy of the first transition states $\mathbf{2_A}$ and $\mathbf{2_{B,C}}$ in Fig. 6), which is consistent with the very low level of methylation verified in this case. In the MeOBuOTs and MeOPenOTs systems, the first energy barrier associated with the pre-organization of a 5- and 6-member ring is smaller in Routes B and C than that in Route A (that is, $\mathbf{2_{B,C}} < \mathbf{2_A}$), although the difference in the energies of the transition states $\mathbf{2_{B,C}}$ and $\mathbf{2_A}$ (of ~6 kJ mol^{-1}) is significantly smaller than the corresponding energy difference for the MeOEtOTs system. However, even this relatively small difference seems to be high enough to contribute, along with other effects discussed later, with the much higher degrees of methylation (Figs. 3 and 4) obtained in these two systems; the difference in energy is approximately equal to 2 *RT*, which, thus, leads to a large effect in the reaction rate constant, given its contribution to Arrhenius' equation exponential factor. Another important point is the decrease in the lowest activation energy of the first step ($\mathbf{1} \rightarrow \mathbf{2}$) as one goes from systems associated with the intermediacy of 3-membered to 5-membered to 6-membered ring species, *i.e.*, MeOEtOTs to MeOBuOTs to MeOPenOTs systems, respectively. Accordingly, on changing from the MeOEtOTs to MeOBuOTs system, a decrease of ~5 kJ mol^{-1} in the activation energy is predicted, while on changing from the MeOBuOTs to the MeOPenOTs system, the activation energy is decreased by a further ~4 kJ mol^{-1} (Fig. 6).

Other important feature in the control of the reaction rates is the probability that a given atom hits the correct atom associated with the desired transformation so that a productive TS is formed. For instance, for the formation of TS $\mathbf{2_A}$ the *N*-atom of the pyridine ring must reach the C-atom directly bound to the tosylate group in MeOalkylOTs (Fig. 5), in order to yield the effective transition state $\mathbf{2_A}$, at the expense of many ineffective collisions with other atoms that give rise to no reaction. Thus, the probability of such favorable encounters and effective collisions decreases as the tosylate side-chain lengthens. Therefore, it is expected that such effect should lead to a further decrease (apart from the influence of the barrier height) in likelihood of structurally organizing the system as required by the transition state $\mathbf{2_A}$ for the five- and six-membered ring systems, *i.e.*, MeOBuOTs and MeOPenOTs systems, respectively, which eventually translates into a reduced effective likelihood of Route A for this longer side-chained tosylates. The difference in the magnitude of such effect between these particular MeOBuOTs and MeOPenOTs systems should be almost negligible, since they differ by just one C-atom out of 6 or 7 core atoms, respectively, in the side chains. This type of statistical effect is also expected to be important for the formation of the transition state $\mathbf{2_{B,C}}$, which involves an intramolecular heterocyclic ring formation (Fig. 5). The number of rotational isomers (minima) of a given chain formed by *N* single bonds is 3^N [52]. In the present case *N* coincides with the number of single bonds in the heterocyclic ring, since only these bonds are important for the ring-closure probability. The population of a given minimum can be connected to its energy, *via* Boltzmann distribution. For MeOBuOTs, the lowest energy minimum is expected to be a precursor of a particular 5-membered ring conformer corresponding to the formation of the TS $\mathbf{2_{B,C}}$ out of a total of 243 possible conformers ($N = 5$). The conformers that resemble precursors of 3- and 4-membered rings in MeOBuOTs are ineffective for yielding the desired reaction (O-atom would hit an internal, non-activated CH_2 group) and, additionally, as a consequence of ring strain [51], their energies should be considerably higher. Thus, despite the fact that they contribute with a relatively large number of conformers, their Boltzmann populations are expected to be small. Therefore, it is reasonable to assume that their occurrence represents an almost negligible obstacle for the formation of TS $\mathbf{2_{B,C}}$. The same holds for MeOPenOTs, as the desired precursor for $\mathbf{2_{B,C}}$ is a 6-membered ring out of 729 possible conformers ($N = 6$) and the energies of the ineffective 5-, 4- and 3-membered ring conformers are higher

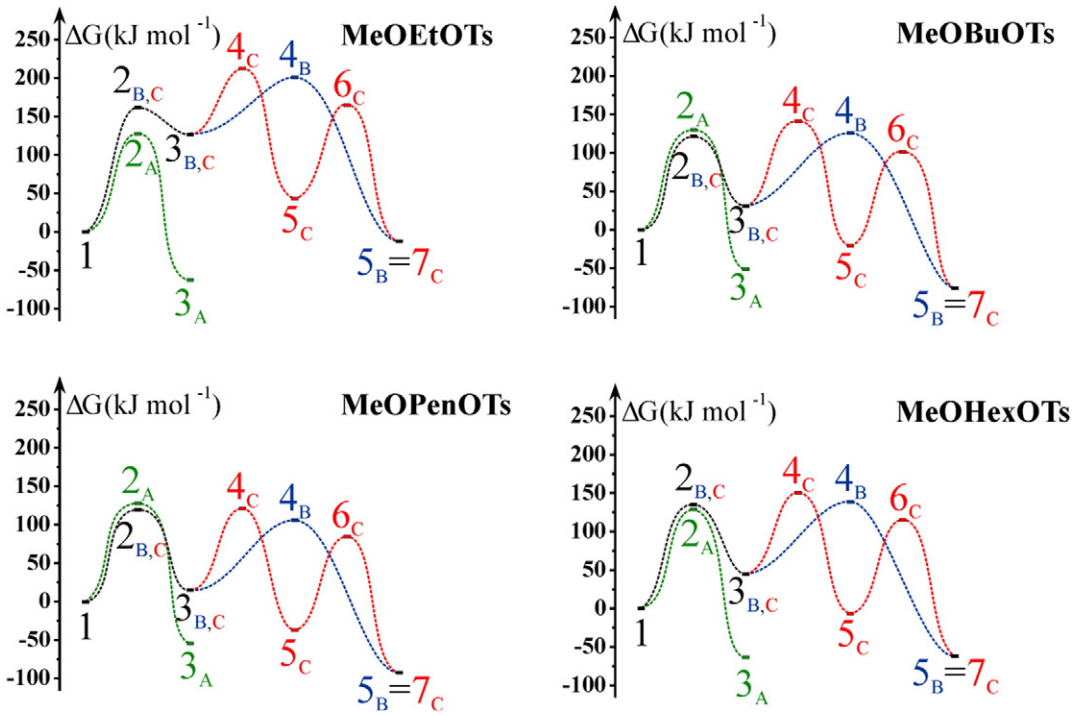

Fig. 6. Gibbs free energy profile calculated at M06-2X/6–311++G(2d,p)//M06-2X/6–31+G(d) DFT level for the species associated with the mechanisms given in Fig. 5. Compression and ionic pair effects were taken into account where appropriate (see text). Actual energy values are listed in the supplementary information material.

and in an ascending order (5-member < 4-member < 3-membered ring). On the other hand, in the case of MeOHexOTs, for which there are 2187 minima ($N = 7$), the desired reaction involves formation of a 7-membered ring, which, of all possible precursor rings, is not the lowest energy ring. Thus, formation of TS $\mathbf{2_{B,C}}$ is difficult given the occurrence of ineffective 6-membered precursor ring conformer that, as a consequence of its lower energy [51], have higher Boltzmann population than the corresponding population of the desired, effective 7-membered ring conformer. Overall, the net effect in the case of MeOHexOTs is to hinder the formation of TS $\mathbf{2_{B,C}}$ in comparison to what would be expected as a consequence of a sole effect of the activation barriers. These combined energetic and conformational factors explain the low level of methylation observed experimentally for this system (Fig. 4), close to that found in the MeEtOTs systems. It is suggested then that the net outcome of the statistical and energy barrier effects makes the effective formation of TS $\mathbf{2_{B,C}}$ in MeOHexOTs as unfavorable as in the case of MeOEtOTs.

Fig. 6 reveals that the formation of product $\mathbf{3_A}$ is thermodynamically more favorable than $\mathbf{5_B}$ for both MeOEtOTs and MeOHexOTs, *i.e.*, the methoxyalkylation route is more favorable than the methylation routes. However, whereas for MeOEtOTs the energy difference between products and reactants is ~50 kJ mol^{-1}, for MeOHexOTs this difference is just ~1 kJ mol^{-1}. Thus, for these two systems, route A (methoxyalkylation) is kinetically, as well as thermodynamically, more favorable than Routes B and C, although the thermodynamic effect is very small for MeOHexOTs. On the other hand, for MeOBuOTs and MeOPenOTs, formation of $\mathbf{5_B}$ is thermodynamically more favorable than formation of $\mathbf{3_A}$ by ~23 and ~37 kJ mol^{-1}, respectively. Therefore, for MeOBuTs and MeOPenOTs, Routes B and C (leading to the methylation reactions) are both kinetically and thermodynamically more favorable than Route A.

For MeOEtOTs, the relative stability between the transition states $\mathbf{4_B}$ and $\mathbf{4_C}$ seems to be of secondary importance, since Routes B and C are avoided already in the first step, related to the formation of $\mathbf{2_{B,C}}$, as the free energy of $\mathbf{2_A}$ is significantly lower than that of $\mathbf{2_{B,C}}$ (Fig. 6). Conversely, the relative stability between the transition states $\mathbf{4_B}$ and $\mathbf{4_C}$ for MeOHexOTs (Fig. 6) may play an important role in hindering the formation of $\mathbf{5_B}$, which is consistent with the low methylation yields observed experimentally (Fig. 4) Despite the fact that such difference (of ~12.8 kJ mol^{-1}) is relatively high, the formation of products $\mathbf{5_C}$ is likely to be non-negligible, thus causing a further decrease in the yield of methylated pyridinium species $\mathbf{5_B}$. Formation of methylation products $\mathbf{5_C}$ in relatively high amounts may be explained by the large excess of MeOalkylOTs used under experimental conditions, as the formation of TS $\mathbf{4_C}$ involves a bimolecular reaction, whose rate depends on the concentration of tosylate. Conversely, the rate of formation of $\mathbf{5_B}$ from TS $\mathbf{4_B}$ is independent of MeOalkylOTs concentration. Additionally, formation of $\mathbf{5_C}$ is also justified by the fact that MeOalkylOTs alone, heated in DMF at 105 °C has been shown experimentally to yield the methylating agent MeOTs. The prevalence of the methylation routes for MeOBuOTs and MeOPenOTs systems in comparison with MeOHexOTs may arise from a further increase of ~2.2 kJ mol^{-1} in the relative stability of TS $\mathbf{4_B}$ *versus* $\mathbf{4_C}$ along with much larger relative thermodynamic stability of $\mathbf{3_A}$ and $\mathbf{5_B}$ (and the other aforementioned effects for MeOHexOTs).

Routes B and C develop through a common methyl oxonium salt as intermediate. The reaction of the methyl oxonium salt with its tosylate counter-ion or with the pyridine (or pyridyl moiety of *N*-pyridylporphyrins) represents the crucial step in defining the overall methylation as a result of Route C or Route B, respectively. The formation of each methyl oxonium cation leads to the concomitant formation of a tosylate anion in close proximity to the cation. The access of pyridine (or *N*-pyridylporphyrin) to the methyl oxonium cation in a timely manner is not necessary granted, given that it depends on the effective diffusion of the pyridine moiety from the solution bulk to the methyl oxonium cation intermediate. Therefore, the reaction of this cation with the tosylate to yield the stable methylating agent MeOTs, which would eventually promote methylation (Route C), should occur at the expense of direct transfer of the methyl moiety from the oxonium cation intermediate to pyridine or *N*-pyridylporphyrin.

The compromised balance among the suggested mechanisms given by Routes A, B, and C to describe the methoxyalkylation *versus* methylation reactions of *N*-pyridylporphyrins is in agreement with experimental data depicted in Figs. 2, 3 and 4, especially when analyzed in

conjunction with the reaction times needed for full quaternization of the porphyrin isomers in various systems. In general, time needed for the completion of the methoxyalkylation reaction of *N*-pyridylporphyrins with 2-methoxyethyl and 6-methoxythexyl chains was similar to that observed with the corresponding alkyl analogues of equivalent chain length [30]. The reactions with MeOBuOTs and MeOPenOTs to yield the fully quaternized MnP mixtures were remarkably faster. For example, reactions of the *ortho N*-pyridylporphyrin with MeOEtOTs and MeOHexOTs lasted, as anticipated, ~24 h, whereas full quaternization with MeOBuOTs and MeOPenOTs was achieved in a remarkably short time frame of 4 h. These shortened reaction times are associated with higher level of methylated species, which deems pyridyl unavailable to methoxyalkylation and leads much rapidly to predominately methylated, but fully quaternized product. Effective collisions between the pyridyl group of an *N*-pyridylporphyrin and the activated CH_2 group of a tosylate becomes statistically less likely as the side-chain lengthens, which should result, under normal condition [30], in slower reactions for longer side-chain tosylates. Conversely, methylations are considerably fast as effective collisions are more likely, given the methylating agent is available. Thus, if the methoxyalkyl tosylate is prone to rearrangement, as in MeOBuOTs and MeOPenOTs, the slow methoxyalkylation allows time for the side-chain reorganization to take place and for the *in situ*-generated methylating agent to accumulate to levels enough to favor methylation at the expense of methoxyalkylation. Such reaction trend results in the methylation profile given in Figs. 3 and 4. It is worth noting that the overall picture indicates that the *N*-pyridylporphyrins are acting as a somewhat exotic trapping reagent and expensive sensor for the *in situ* formation of methylating agents in these methoxyalkyl tosylate systems.

3.3. MnTnBuOE-2-PyP^{5+}

The studies of the methoxyalkyl tosylate systems paved way for the successful synthesis of the Mn(III) 2-*N*-pyridyl porphyrin derivative bearing butoxyethyl side-chains, MnTnBuOE-2-PyP^{5+} (BMX-001) (Fig. 1). This compound is now in Phase I/II Clinical Trial at Duke University, USA (see additional information under Final Remarks). The design of this compound explored the fact that the placement of the oxygen atom closer to the sulfonato group in alkoxyethyltosylate would, by analogy to the methoxyethyl tosylate system, disfavor rearrangement of the tosylate and favor, thus, alkoxyethylation versus alkylation. Indeed, the synthesis of MnTnBuOE-2-PyP^{5+} was accomplished [44] with no signs of competing butylation reaction. DFT calculations on competing Routes A, B, and C for the butoxyethyl tosylate system yielded energy profiles that were remarkably similar to those of the MeOEtOTs system, except that nBuOEtOTs-based n-butylation is even slightly disfavored than MeOEtOTs-based methylation (Fig. 7). By keeping the oxygen atom 2 carbons away from the sulfonato group, formation of a 3 membered-ring as an intermediate in Routes B and C is highly disfavored, and the desired butoxyethylation reaction (Route A) is the major pathway leading to MnTnBuOE-2-PyP^{5+}. The overall profile of MeOEtOTs and nBuOEtOTs are, thus, in excellent agreement with experimental reactivity trend.

It is worth noting that whereas MeOPenOTs and nBuOEtOTs are isomers of identical chain length, the relative position of oxygen atom within the chain places these two compounds on the very opposite sides of the reactivity trend: MeOPenOTs being extremely prone to rearrangement and favoring the corresponding methylation pathways (via Routes B and/or C), while nBuOEtOTs reacts in its own right, favoring butoxyethylation products (Route A).

Aside from the impact on the reactivity pattern of the tosylate, the relative position of the oxygen atom is also of outmost importance in controlling and defining the lipophilicity of the resulting MnP complex. The extent of solvation of the systems in which the oxygen atoms are exposed (at the end of the side-chains) relative to those buried deeply within the chains is greatly different. Whereas the methoxyhexyl derivatives are relatively hydrophilic [53], the butoxyethyl analogue, MnTnBuOE-2-PyP^{5+}, is not only lipophilic but exhibit also low surfactancy character and low toxicity [44]. With 4 cationic nitrogens, the anticipated high Mn(III)/Mn(II) reduction potential ($E_{½}$) and the high SOD-like activity were demonstrated [44].

3.4. Reevaluation of the purity/identity of MnTMOE-2-PyP^{5+} and MnTTEG-2-PyP^{5+} preparations

Understanding the mechanism of quaternization with oxygen-bearing *p*-toluenesulfonates allowed us not only to design and optimize the structure of SOD mimics, but to revisit and accurately identify the main product and by-products in the preparations of other SOD mimics and peroxynitrite scavengers reported by us, *i.e.*, MnTMOE-2-PyP^{5+} and Mn PEG-ylated porphyrin (MnTTEG-2-PyP^{5+}) [25,26], and to speculate on the composition of the Fe PEG-ylated analogue, FP-15, prepared by others [54,55]. While we have not tested the efficacy of MnTMOE-2-PyP^{5+} and MnTTEG-2-PyP^{5+} *in vivo* (other than in *E. coli* study), FP-15 has been used in different animal models [54–56]. At the point we originally reported the identity and purity of our preparations of MnTMOE-2-PyP^{5+} and MnTTEG-2-PyP^{5+} we had not yet established an ESI-MS conditions which would have prevented analyte fragmentation. Thus we assigned then [25,26], the multiple peaks in mass spectra to fragmentation and losses at the ESI-MS ionization chamber, which hampered the identification of MnP contaminants in the isolated materials. With the use of heptafluorobutyric acid as an ESI-MS additive to allow ion pairing and prevent MnP fragmentation [32], the situation with the formerly called MnTMOE-2-PyP^{5+} sample was clarified in the present work: Fig. 3 indicates that the isolated preparation is, in fact, a mixture of fully quaternized MnPs in which the target MnTMOE-2-PyP^{5+} compound amounts to ~70% and the remaining ~30% relates to MnP^{5+} species with one or two methoxyethyl moieties being replaced by methyl groups (Fig. 3).

The revisited ESI-MS analysis of the Mn PEG-ylated compound revealed a fair number of by-products; the FP-15 which differs from MnTTEG-2-PyP^{5+} only by having Fe instead of Mn as the metal center, should likewise contain the analogous porphyrin-based impurities/byproducts [54–56]. Due to the formation of cycles of different length during quaternization, the preparations of MnTTEG-2-PyP^{5+} contains not only the compound of interest, but species with different alkyl and alkoxyalkylpyridyl substituents (Table 1). Whereas all by-products must be SOD active (given the structure-activity relationships devised for cationic porphyrins) [57–59], they likely have significantly different lipophilicities and therefore bioavailabilities which should affect considerably their *in vivo* efficacy [1,2,4–6].

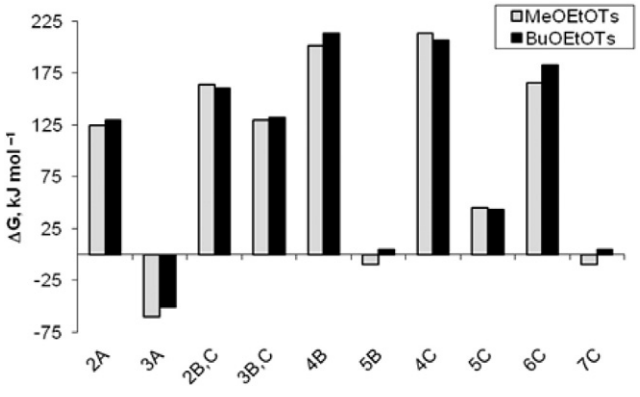

Fig. 7. Comparison of the Gibbs free energy for the MeOEtOTs and nBuOEtOTs systems calculated at M06-2X/6–311++G(2d,p)//M06-2X/6–31+G(d) DFT level for the species associated with the mechanisms given in Fig. 5. Compression and ionic pair effects were taken into account where appropriate (see text). Actual energy values are listed in Supplementary Information.

4. Final remarks

The remarkable therapeutic efficacy of early cationic Mn(III) *N*-substituted pyridylporphyrins prompted us to optimize their structure to maintain high redox properties along with high bioavailability and low toxicity. A possible strategy was to introduce oxygen atoms into pyridyl *N*-alkyl substituents; such approach however imposed synthetic challenges. A systematic evaluation of the interaction of *ortho*, *meta*, *para* Mn(III) *N*-pyridylporphyrins with alkoxyalkyl tosylates indicated what type of oxygen-bearing analogues could be synthesized in purity compatible with biological demands. MnTnBuOE-2-PyP^{5+} emerged from such studies and is presently in Clinical Trial as a radioprotector of normal brain with high-grade glioma patients at Duke University (NCT02655601). Another trial on radioprotection of salivary glands and mouth mucosa will commence in early 2017 on head and neck cancer patients jointly at Duke University and University of Colorado (USA, NCT02990468).

In brief our studies reported herein demonstrated that *N*-methylated pyridyl species in *N*-methoxyalkylpyridylporphyrins originate from unanticipated rearrangement mechanisms rather than from impurities in *p*-toluenesulfonate, solvent or starting non-alkylated porphyrin. The possibility of preparing reasonably pure (>95%) *meta* *N*-pyridylporphyrins fully quaternized with 4-methoxybutyl and 5-methoxypentyl substituents was abandoned, as well as the synthesis of *ortho* and *para* *N*-methoxyalkylpyridylporphyrins. Our studies on the mechanism of *N*-alkoxyalkyl derivatization of porphyrin pyridyls led to the synthesis of MnTnBuOE-2-PyP^{5+} and prove that the instability associated with the formation of small 3-membered ring minimized the likelihood of butoxyethyl tosylate side-chain rearrangement and consequent formation of undesired by-products. The compound retains the powerful redox properties of analogous *ortho* MnP^{5+} and, as anticipated, is 4–5-fold less toxic due to the oxygen atoms disrupting micellar properties of analogous alkyl chains [44]. The previous success on the synthesis of hexoxyethyl analogue, MnTnHexOE-2-PyP^{5+} [29], is also explained by the unfavorable three-membered ring formation during quaternization leading to the isolation of a compound of as high purity as that of MnTnBuOE-2-PyP^{5+} [29,44]. The knowledge obtained herein is invaluable for the synthesis of *N*-alkoxyalkylpyridylporphyrins with oxygen-atom as close to the pyridyl groups as possible to minimize the competing tosylate rearrangements and the formation of unwanted species that may lead to undesired alkylated products.

Acknowledgement

The authors are thankful to Duke University's CTSA grant 1 UL 1 RR024128-01 from NCRR/NIH (AT, IBH, IS), NIH/NCI Duke Comprehensive Cancer Center Core Grant (5-P30-CA14236-29) (IS), NIH 1R03-NS082704-01 (AT, IS and IBH), and IBH general research funds (AT). OLS, INP, SAM, EV, and JSR thank funding from CNPq, CAPES, and FINEP. National Center for High Performance Computing in São Paulo (CENAPAD-SP, Campinas, Brazil) is greatly acknowledged. Ezequiel F.V. Leitão is thanked for help with preparation of Fig. 6.

Table 1
Electrospray ionization mass spectrometry data for MnTTEG-2-PyP^{5+}.

MnTTEG-2-PyP^{5+} species	*m/z* [found (calculated)]
(4PEG + HFBA$^-$)$^{4+}$/4	368.4 (368.1)
(1PEG/3Me + 2HFBA$^-$)$^{3+}$/3	430.2 (429.8)
(1PEG/2Me/1MeOEt + 2HFBA$^-$)$^{3+}$/3	445.0 (444.4)
(2PEG/2Me + 2HFBA$^-$)$^{3+}$/3	473.9 (473.8)
(2PEG/1Me/1MeOEt + 2HFBA$^-$)$^{3+}$/3	488.9 (488.5)
(3PEG/1Me + 2HFBA$^-$)$^{3+}$/3	518.0 (517.8)
(3PEG/1MeOEt + 2HFBA$^-$)$^{3+}$/3	533.0 (532.5)
(4PEG + 2HFBA$^-$)$^{3+}$/3	562.3 (561.8)
(4PEG + 3HFBA$^-$)$^{3+}$/2	949.7 (549.0)

~1 μM solution of MnTTEG-2-PyP^{5+} in 1:1 v/v acetonitrile:H_2O (containing 0.01% v/v heptafluorobutyric acid (HFBA)) mixture, 20 V cone voltage.

Appendix A. Supplementary data

Supplementary data to this article can be found online at http://dx.doi.org/10.1016/j.jinorgbio.2017.01.003.

References

[1] I. Batinic-Haberle, Z. Rajic, A. Tovmasyan, J.S. Reboucas, X. Ye, K.W. Leong, M.W. Dewhirst, Z. Vujaskovic, L. Benov, I. Spasojevic, Free Radic. Biol. Med. 51 (2011) 1035–1053.
[2] I. Batinic-Haberle, J.S. Reboucas, L. Benov, I. Spasojevic, in: K.M. Kadish, K.M. Smith, R. Guillard (Eds.), Handbook of Porphyrin Science, vol. 11, World Scientific, Singapore 2011, pp. 291–393.
[3] I. Batinic-Haberle, J.S. Reboucas, I. Spasojevic, Antioxid. Redox Signal. 13 (2010) 877–918.
[4] I. Batinic-Haberle, I. Spasojevic, H.M. Tse, A. Tovmasyan, Z. Rajic, D.K.S. Clair, Z. Vujaskovic, M.W. Dewhirst, J.D. Piganelli, Amino Acids 42 (2012) 95–113.
[5] I. Batinic-Haberle, A. Tovmasyan, E.R. Roberts, Z. Vujaskovic, K.W. Leong, I. Spasojevic, Antioxid. Redox Signal. 20 (2014) 2372–2415.
[6] I. Batinic-Haberle, A. Tovmasyan, I. Spasojevic, Redox Biol. 5 (2015) 43–65.
[7] S. Miriyala, I. Spasojevic, A. Tovmasyan, D. Salvemini, Z. Vujaskovic, D.S. Clair, I. Batinic-Haberle, Biochim. Biophys. Acta 2012 (1822) 794–814.
[8] A. Tovmasyan, H. Sheng, T. Weitner, A. Arulpragasam, M. Lu, D.S. Warner, Z. Vujaskovic, I. Spasojevic, I. Batinic-Haberle, Medical principles and practice: International Journal of the Kuwait University, Health Sci. Cent. 22 (2013) 103–130.
[9] I. Batinic-Haberle, L. Benov, I. Spasojevic, I. Fridovich, J. Biol. Chem. 273 (1998) 24521–24528.
[10] I. Batinić-Haberle, I. Spasojević, P. Hambright, L. Benov, A.L. Crumbliss, I. Fridovich, Inorg. Chem. 38 (1999) 4011–4022.
[11] I. Kos, L. Benov, I. Spasojevic, J.S. Reboucas, I. Batinic-Haberle, J. Med. Chem. 52 (2009) 7868–7872.
[12] I. Kos, J.S. Reboucas, G. DeFreitas-Silva, D. Salvemini, Z. Vujaskovic, M.W. Dewhirst, I. Spasojevic, I. Batinic-Haberle, Free Radic. Biol. Med. 47 (2009) 72–78.
[13] I. Spasojevic, Y. Chen, T.J. Noel, P. Fan, L. Zhang, J.S. Reboucas, D.K.S. Clair, I. Batinic-Haberle, Free Radic. Biol. Med. 45 (2008) 943–949.
[14] I. Spasojevic, I. Kos, L.T. Benov, Z. Rajic, D. Fels, C. Dedeugd, X. Ye, Z. Vujaskovic, J.S. Reboucas, K.W. Leong, M.W. Dewhirst, I. Batinic-Haberle, Free Radic. Res. 45 (2011) 188–200.
[15] I. Spasojevic, T. Weitner, A. Tovmasyan, H. Sheng, S. Miriyala, D. Leu, Z. Rajic, D.S. Warner, D.S. Clair, T.-T. Huang, I. Batinic-Haberle, Free Radic. Biol. Med. 65 (2013) S132.
[16] T. Weitner, I. Kos, H. Sheng, A. Tovmasyan, J.S. Reboucas, P. Fan, D.S. Warner, Z. Vujaskovic, I. Batinic-Haberle, I. Spasojevic, Free Radic. Biol. Med. 58 (2013) 73–80.
[17] I. Spasojevic, Y. Chen, T.J. Noel, Y. Yu, M.P. Cole, L. Zhang, Y. Zhao, D.K.S. Clair, I. Batinic-Haberle, Free Radic. Biol. Med. 42 (2007) 1193–1200.
[18] I. Spasojevic, A. Li, A. Tovmasyan, Z. Rajic, D. Salvemini, D.S. Clair, J.S. Valentine, Z. Vujaskovic, E.B. Gralla, I. Batinic-Haberle, Free Radic. Biol. Med. 49 (2010) S199.
[19] I. Spasojevic, S. Miriyala, A. Tovmasyan, D. Salvemini, Z. Vujaskovic, I. Batinic-Haberle, D.S. Clair, Free Radic. Biol. Med. 51 (2011) S98.
[20] Z. Okun, Z. Gross, Inorg. Chem. 51 (2012) 8083–8090.
[21] A. Tovmasyan, T. Weitner, H. Sheng, M. Lu, Z. Rajic, D.S. Warner, I. Spasojevic, J.S. Reboucas, L. Benov, I. Batinic-Haberle, Inorg. Chem. 52 (2013) 5677–5691.
[22] S.C. Gad, D.W. Sullivan Jr., J.D. Crapo, C.B. Spainhour, Int. J. Toxicol. 32 (2013) 274–287.
[23] S.C. Gad, D.W. Sullivan Jr., I. Spasojevic, C.V. Mujer, C.B. Spainhour, J.D. Crapo, Int. J. Toxicol. (2016)http://dx.doi.org/10.1177/1091581816642766.
[24] K.A. Ashcraft, M.K. Boss, A. Tovmasyan, K. Roy Choudhury, A.N. Fontanella, K.H. Young, G.M. Palmer, S.R. Birer, C.D. Landon, W. Park, S.K. Das, T. Weitner, H. Sheng, D.S. Warner, D.M. Brizel, I. Spasojevic, I. Batinic-Haberle, M.W. Dewhirst, Int. J. Radiat. Oncol. Biol. Phys. 93 (2015) 892–900.
[25] I. Batinic-Haberle, I. Spasojevic, R.D. Stevens, B. Bondurant, A. Okado-Matsumoto, I. Fridovich, Z. Vujaskovic, M.W. Dewhirst, Dalton Trans. (2006) 617–624, http://dx.doi.org/10.1039/b513761f.
[26] I. Batinic-Haberle, I. Spasojevic, R.D. Stevens, P. Hambright, P. Neta, A. Okado-Matsumoto, I. Fridovich, Dalton Trans. (2004) 1696–1702, http://dx.doi.org/10.1039/b400818a.
[27] I.U. Rau, M. Rehahn, Acta Polym. 45 (1994) 3–13.
[28] R.S. Tipson, J. Org. Chem. 9 (1944) 235–241.
[29] A. Tovmasyan, S. Carballal, R. Ghazaryan, L. Melikyan, T. Weitner, C.G. Maia, J.S. Reboucas, R. Radi, I. Spasojevic, L. Benov, I. Batinic-Haberle, Inorg. Chem. 53 (2014) 11467–11483.
[30] I. Batinić-Haberle, I. Spasojević, R.D. Stevens, P. Hambright, I. Fridovich, Dalton Trans. (2002) 2689–2696.
[31] V.H. Pinto, D. Carvalhoda-Silva, J.L. Santos, T. Weitner, M.G. Fonseca, M.I. Yoshida, Y.M. Idemori, I. Batinic-Haberle, J.S. Reboucas, J. Pharm. Biomed. Anal. 73 (2013) 29–34.
[32] J.S. Reboucas, I. Spasojevic, I. Batinic-Haberle, J. Pharm. Biomed. Anal. 48 (2008) 1046–1049.
[33] T. Clark, J. Chandrasekhar, G.W. Spitznagel, P.V. Schleyer, J. Comput. Chem. 4 (1983) 294–301.
[34] U.A. Frank, J.M. Bordiuk, V. Borromeo-McGrail, M.B. Saltzman, H.G. Keitel, Pediatrics 51 (1973) 878–883.
[35] P.M.W. Gill, B.G. Johnson, J.A. Pople, M.J. Frisch, Chem. Phys. Lett. 197 (1992) 499–505.

[36] P. Harihara, J.A. Pople, Theor. Chim. Acta 28 (1973) 213–222.
[37] R. Krishnan, J.S. Binkley, R. Seeger, J.A. Pople, J. Chem. Phys. 72 (1980) 650–654.
[38] A.D. Mclean, G.S. Chandler, J. Chem. Phys. 72 (1980) 5639–5648.
[39] M. J. Frisch, G. W. Trucks, H. B. Schlegel, G. E. Scuseria, M. A. Robb, J. R. Cheeseman, G. Scalmani, V. Barone, B. Mennucci, G. A. Petersson, H. Nakatsuji, M. Caricato, X. Li, H. P. Hratchian, A. F. Izmaylov, J. Bloino, G. Zheng, J. L. Sonnenberg, M. Hada, M. Ehara, K. Toyota, R. Fukuda, J. Hasegawa, M. Ishida, T. Nakajima, Y. Honda, O. Kitao, H. Nakai, T. Vreven, J. Montgomery, J. A., J. E. Peralta, F. Ogliaro, M. Bearpark, J. J. Heyd, E. Brothers, K. N. Kudin, V. N. Staroverov, R. Kobayashi, J. Normand, K. Raghavachari, A. Rendell, J. C. Burant, S. S. Iyengar, J. Tomasi, M. Cossi, N. Rega, N. J. Millam, M. Klene, J. E. Knox, J. B. Cross, V. Bakken, C. Adamo, J. Jaramillo, R. Gomperts, R. E. Stratmann, O. Yazyev, A. J. Austin, R. Cammi, C. Pomelli, J. W. Ochterski, R. L. Martin, K. Morokuma, V. G. Zakrzewski, G. A. Voth, P. Salvador, J. J. Dannenberg, S. Dapprich, A. D. Daniels, O. Farkas, J. B. Foresman, J. V. Ortiz, J. Cioslowski and D. J. Fox, Gaussian, Inc.: Wallingford, CT, 2010.
[40] M. Cossi, N. Rega, G. Scalmani, V. Barone, J. Comput. Chem. 24 (2003) 669–681.
[41] M.A. Kastenholz, P.H. Hunenberger, J. Chem. Phys. 124 (2006) 224501.
[42] A. Ben-Naim, Solvation thermodynamics, Springer US, 1987.
[43] J.L. Pascual-ahuir, E. Silla, I. Tuñon, J. Comput. Chem. 15 (1994) 1127–1138.
[44] Z. Rajic, A. Tovmasyan, I. Spasojevic, H. Sheng, M. Lu, A.M. Li, E.B. Gralla, D.S. Warner, L. Benov, I. Batinic-Haberle, Free Radic. Biol. Med. 52 (2012) 1828–1834.
[45] L.G. Donaruma, J. Org. Chem. 22 (1957) 1024–1029.
[46] Y. Zhao, D.G. Truhlar, Theor. Chem. Accounts 120 (2008) 215–241.
[47] M. Dracinsky, P. Jansa, J. Chocholousova, J. Vacek, S. Kovackova, A. Holy, Eur. J. Org. Chem. (2011) 777–785, http://dx.doi.org/10.1002/ejoc.201001335.
[48] R. Lazny, A. Ratkiewicz, A. Nodzewska, J. Wysocka, Tetrahedron Lett. 53 (2012) 5871–5874.
[49] J.R. Pliego Jr., Phys. Chem. Chem. Phys. 13 (2011) 779–782.
[50] C.P. Kelly, C.J. Cramer, D.G. Truhlar, J. Phys. Chem. B 111 (2007) 408–422.
[51] T. Dudev, C. Lim, J. Am. Chem. Soc. 120 (1998) 4450–4458.
[52] E.I. Izgorodina, C. Yeh Lin, M.L. Coote, Phys. Chem. Chem. Phys. 9 (2007) 2507–2516.
[53] A.G. Tovmasyan, Z. Rajic, I. Spasojevic, J.S. Reboucas, X. Chen, D. Salvemini, H. Sheng, D.S. Warner, L. Benov, I. Batinic-Haberle, Dalton Trans. 40 (2011) 4111–4121.
[54] T. Radovits, C.J. Beller, J.T. Groves, B. Merkely, M. Karck, C. Szabo, G. Szabo, Eur. J. Cardiothorac. Surg. 41 (2012) 391–396.
[55] T. Radovits, L. Seres, D. Gero, L.N. Lin, C.J. Beller, S.H. Chen, J. Zotkina, I. Berger, J.T. Groves, C. Szabo, G. Szabo, Mech. Ageing Dev. 128 (2007) 173–181.
[56] C. Szabo, J.G. Mabley, S.M. Moeller, R. Shimanovich, P. Pacher, L. Virag, F.G. Soriano, J.H. Van Duzer, W. Williams, A.L. Salzman, J.T. Groves, Mol. Med. 8 (2002) 571–580.
[57] J.S. Reboucas, G. DeFreitas-Silva, I. Spasojevic, Y.M. Idemori, L. Benov, I. Batinic-Haberle, Free Radic. Biol. Med. 45 (2008) 201–210.
[58] I. Batinic-Haberle, A. Tovmasyan, Superoxide dismutase mimics and other redox-active therapeutics, in: D Armstrong, RD Stratton (Eds.), Oxidative stress and antioxidant protection:The science of free radical biology and disease, Wiley, New York 2016, pp. 415–470.
[59] I. Batinic-Haberle, A. Tovmasyan, I. Spasojevic, Mn porphyrin-based redox-active therapeutics" in Book "Redox-Active Therapeutics", Batinic-Haberle, Reboucas, Spasojevic (Eds.),© Springer International Publishing Switzerland (2016) 165–211, http://dx.doi.org/10.1007/978-3-319-30705-3_8.